Error Characteristics of Ceilometer-Based Observations of Cloud Amount

TIMOTHY J. WAGNER

Cooperative Institute for Meteorological Satellite Studies, Space Science and Engineering Center, University of Wisconsin–Madison, Madison, Wisconsin

JESSICA M. KLEISS

Environmental Studies Program, Lewis and Clark College, Portland, Oregon

(Manuscript received 21 December 2015, in final form 28 April 2016)

ABSTRACT

Ceilometer observations of cloud cover are an important component of the automated weather observation network. However, the accuracy of its measurements of cloud amount is impacted by the limited vertical range and areal extent of its observations. A multiyear collocated dataset of observations from a laser ceilometer, a total sky imager (TSI), and a micropulse lidar (MPL) at the Atmospheric Radiation Measurement (ARM) Southern Great Plains (SGP) Central Facility is used to simulate the observations of operational ceilometers and to analyze the magnitude of the errors associated with ceilometer-based observations of cloud amount. The limited areal coverage of ceilometers results in error when skies are heterogeneous, but these errors are small compared to those caused by the limited vertical range: observations of clear sky or few clouds are often in error as the instrument cannot detect the presence of upper-level clouds. The varying quantities of upper-level clouds mean that errors are diurnally and seasonally dependent, with the greatest error at the SGP site happening in the morning and summer, respectively. Overall, the spatial homogeneity and low base of stratus clouds means that ceilometer-based observations of overcast skies are the most accurate, with a root-mean-square error of cloud fraction in overcast conditions an order of magnitude lower than for the dataset as a whole.

1. Introduction

Because of their significant impact on radiative and latent heat fluxes in the troposphere, clouds play an important role in modulating atmospheric conditions. The effects of clouds can be ascertained on a variety of spatial and temporal scales, from impacting daily temperature extremes to modifying the climatological norms for a particular region. The importance of clouds to the climate system has been reaffirmed by the Intergovernmental Panel on Climate Change (IPCC) Fifth Assessment Report (AR5), which notes that they remain the single greatest source of uncertainty in estimating the magnitude of changes to the energy budget of the planet (Boucher et al. 2013). It is readily apparent that the accuracy of the simulations performed in weather and climate models fundamentally depends on the ability to properly model clouds and their impacts. While certain cloud species are large enough to be resolved by the current generation of operational weather forecast models, other types, especially convective clouds, are subgrid-scale phenomena and therefore they must be parameterized so that their impact can be ascertained in the absence of direct simulation.

Cloud observations are integral to the improvement of weather and climate models as they provide important information for the development and verification of new models and parameterization schemes. In addition, routine observations of clouds are crucial for operational forecasters, who need to constantly assess the impact of clouds on local radiative and thermodynamic conditions. The aviation community also has a strong interest in quantifying the locations and heights of clouds. Of particular interest to all these communities is the sky cover, or the fractional area of the celestial hemisphere that is covered (but not necessarily obscured, as in the case of thin cirrus) by visible clouds. This differs subtly from cloud fraction, or the nadir view of cloud obscuration, in

Corresponding author address: Timothy J. Wagner, CIMSS, 1225 W Dayton St., Madison, WI 53706.
E-mail: tim.wagner@ssec.wisc.edu

DOI: 10.1175/JTECH-D-15-0258.1

that sky cover is impacted by the curvature of the sky as seen from an observation point on the earth's surface.

Prior to the 1990s, sky cover observations in the United States were taken by human observers, who recorded the fraction in units of oktas (eighths) or tenths, depending on jurisdiction. This is an inherently subjective observation that could be impacted by such factors as the wideness of the sky view and the uneven illumination of the cloud deck at night from the surface (WMO 1975; Hahn et al. 1995). Further bias of the sky cover observation happens at low elevation angles, where the observer sees the sides of the clouds instead of the gaps between them, thus increasing the apparent sky cover fraction (Kassianov et al. 2003). A need to modernize weather observations while reducing ongoing costs led toward the creation of networks of automated weather stations, including today's Automated Surface Observing System (ASOS).

Key to automating the observations of sky cover was the deployment of ceilometers (Dai et al. 2006). Ceilometers emit near-infrared pulses of light, and backscatter by cloud droplets reflects a portion of this energy back toward the surface. As the pulses travel at a known speed, the delay between emission and reception of the pulses can be used to calculate the height of the cloud base. Additional weaker returns from greater distances can indicate the presence of multiple cloud bases. These observations can be used to calculate sky cover by averaging the binary cloud state over a particular period of time. For example, if 50% of the ceilometer observations over a particular period of time contain at least one cloud base, then it is assumed that the sky is 50% covered by clouds.

The current sky cover algorithm in operational use by ASOS installations averages samples taken every 30 s over a 30-min observation time, with the most recent 10 min double weighted in the average (Nadolski 1998), allowing the system to account for rapidly changing environments. Sky cover is assigned to one of a number of categories for the purposes of recording and transmitting the observation in METAR format; the definitions of these categories loosely correspond to classic definitions used during the days of human observations. In order of increasing cloudiness, the categories are clear (CLR, less than or equal to 5% cloudiness), few (FEW, greater than 5% and less than or equal to 25%), scattered (SCT, greater than 25% and less than or equal to 50%), broken (BKN, greater than 50% and less than or equal to 87%), and overcast (OVC, more than 87%). It is important to note that these categories are not equally sized; a broken cloud field can encompass a larger range of possible sky cover fractions than a scattered cloud field, for example. The fraction according to these categories in the METAR format is referred to as the cloud amount, consistent with Nadolski (1998).

While ceilometers represent a more objective method of measuring cloud amount than human observers, it is not without limitations. Fundamentally, the human-based and ceilometer observations are operating in different measurement spaces: the two spatial dimensions that comprise sky cover are approximated by a binary observation (cloud or not cloud) integrated over a temporal dimension. As a result, the sky cover will be recorded as clear even if clouds are present so long as none of them propagates over the ceilometer's line of sight. Furthermore, the temporal averaging present in ceilometer-based observations means that the reported state of the sky is influenced by conditions that may no longer be present; a ceilometer may record an observation of scattered clouds when the sky is completely overcast if a cloud deck rapidly moved into position over the observing site during the averaging period. Finally, the operational ceilometer network is insensitive to high clouds. The ceilometer model that is currently deployed nationwide is capable of retrieving cloud bases up to 7700 m (25 kft) above ground level (AGL), but observations are recorded only if the cloud base is 3660 m (12 kft) AGL or less. This means that despite the significant impact that cirrus clouds have on the radiative budget (Liou 1986), they are currently being ignored by the operational weather observation network due to their excessive height.

Field and process studies have found ceilometer observations were lower than manual observations of sky cover, attributed to the observation of cloud sides near the horizon (Bretherton et al. 1995) and the lack of upper-level cloud observations by the ceilometer (Dai et al. 2006). However, Schreiner et al. (1993) found a favorable comparison when ceilometer observations were merged with geostationary satellite infrared observations of upper-level clouds. Wu et al. (2014) and Boers et al. (2010) combined ceilometers with ground-based active radars and found that the combined product resulted in a higher cloud fraction due to the sensitivity to high thin clouds. This is also consistent with previous reports by Rodriguez (1998) and Rodriguez and Krueger (1999).

Because ceilometers have a relatively low cost, a low need for maintenance, and are capable of observing at all hours, they will remain the primary way that sky cover is observed for the foreseeable future. It is important, however, that the sources and magnitude of errors and biases in the ASOS ceilometer-based sky cover observations are quantified; these topics are the focus of this paper. Through the use of collocated instrumentation, the causes of error in ceilometer observations can be isolated and evaluated independently. This shared record facilitates reevaluation of the algorithms, implicit

assumptions, and error characteristics of the operational automated ceilometer network. While, as outlined above, other studies have conducted intercomparisons between various automated methods of retrieving sky cover, the present work characterizes and quantifies the errors associated with ceilometer-based observations in the context of the operational METAR categories that form the bulk of the climatological record of sky cover in the United States. By better understanding the sky conditions in which ceilometer performance is best as opposed to those with greater uncertainty, characterization of the observations in future meteorological and climatological analyses will be improved and operational forecasters will better understand the accuracies and limitations of the data they routinely utilize.

2. Instrumentation

The Atmospheric Radiation Measurement (ARM; Stokes and Schwartz 1994) Southern Great Plains (SGP) Central Facility houses numerous ground-based remote sensing instruments capable of retrieving observations of clear and cloudy atmospheres. One of the most significant roles that the SGP facility plays is its utility for long-term study of the atmosphere; a ceilometer has been deployed and continuously recording data since late 1997. The location in north-central Oklahoma is exposed to a varying amount of cloudiness over the annual cycle. Lazarus et al. (2000) created a cloud climatology for the SGP site and found that average cloudiness reached a maximum in early spring and a minimum in early summer. Low clouds are more common in winter than in other seasons, midlevel clouds have little variability, and high clouds are less common in fall and winter than they are in spring and summer. Furthermore, it was determined that stratiform clouds are much more common in winter than in other seasons, while convective clouds tend to be found in spring and summer. Additional climatologies (Dong et al. 2005; Dong et al. 2006) have found similar traits of clouds at the SGP site by observing the variability in downwelling radiation. A truly robust sky cover measurement system will need to be able to accurately measure these disparate conditions.

A Vaisala laser ceilometer (CEIL) has been operational at the SGP Central Facility since 2001. This ceilometer can sense cloud presence at up to three separate levels up to a height of 7700 m (25 000 ft) with 10-m vertical resolution. It has a field-of-view divergence of ± 0.83 mrad, resulting in a footprint diameter of 12.8 m at the maximum height of 7700 m (Morris 2012). To accurately simulate the range limitations of ASOS observations, this paper utilizes a modified dataset: all CEIL observations with cloud bases in excess of 3660 m were changed from cloudy to clear.

To properly determine the impact of the ceilometer height limits on observational accuracy of sky cover, it is necessary to compare these observations to a similar instrument with greater vertical range. The micropulse lidar (MPL) is an eye-safe ground-based lidar that operates at 532 nm and is capable of observing cloud-base heights up to 20 km (Wang and Sassen 2001). This instrument provides a dataset of sky cover observations that is qualitatively similar to that of the ceilometer; however, with over 5 times the vertical range, it is capable of observing clouds that cannot be detected by the ceilometer.

3. Comparison to whole-sky imaging

Another automated method of observing sky cover is through digital image processing of sky-view cameras (Pfister et al. 2003; Long et al. 2006; Cazorla et al. 2008; Shields et al. 2013). These are cameras that use various methods such as ultrawide-angle lenses or mirrored domes to capture the entire celestial hemisphere. One common instrument is the total sky imager (TSI; Long et al. 2006), a digital camera suspended over a mirrored dome that reflects the entire sky. A small swath of the dome is marked in nonreflective black. The dome rotates during the day so that the black band is always directed toward the sun, which prevents the imaging chip inside the camera from being saturated and damaged by the sun. Every time the camera photographs the dome, it captures a horizon-to-horizon view of the sky in all directions.

Cloudy and clear regions in TSI images can be detected through digital image processing. A common segmentation procedure considers the ratio of the red to blue channel for each pixel. Since clouds tend to scatter all wavelengths equally, the red–blue ratio is close to unity for cloudy regions. However, as the clear sky is strongly dominated by Rayleigh scattering, it is predominantly blue and the red–blue ratio is less than unity. A threshold on the red–blue ratio is determined as a function of the pixel angle to nadir, angle to the sun, and the solar zenith angle (Koehler et al. 1991). This threshold varies for each imaging apparatus and geographical setting; multiple thresholds can be used to discriminate between clear, thin cloud, and opaque cloud pixels (Long et al. 2006). The sky cover is simply calculated as the ratio of the number of cloudy pixels to the total number of sky pixels. An operational algorithm ingests the TSI imagery and produces quantitative values for sky cover for both thin and opaque clouds, as well as images showing the regions of the sky that have been classified as cloudy or clear. Observations are obtained every 30 s throughout the daylight hours. In this study, the thin and opaque sky covers were combined to produce a total sky cover to be compared to the ceilometer.

As with the other methods of sky cover measurement, there are limitations associated with this method. Of primary importance is the fact that the camera housed within the TSI is sensitive to visible wavelengths only, thus limiting observations to daytime hours. In addition, the TSI requires frequent cleaning to remove dust, bird droppings, and other artifacts that may collect on the mirrored surface. The instrument is designed to withstand all weather conditions, although raindrops and snowflakes on the mirror can interfere with the processing algorithms. Finally, just like a human observer, the TSI is susceptible to the view of cloud sides at large zenith angle. Comparisons of ceilometer to sky camera cloud cover have identified scatter in the comparisons, without necessarily a bias. Boers et al. (2010) found that 17% of the collocated ceilometer–TSI observations exhibited a difference greater than 2 octas. This was the most variability among the five instruments compared. Wacker et al. (2015) found that 24% of the data differed in cloud amount by more than 2 octas. Bretherton et al. (1995) also found significant scatter and a low correlation coefficient of 0.5, but no bias when ceilometer observations were compared to visible *NOAA-12* satellite observations. Note that these three studies used ceilometers with a longer vertical range than the standard ASOS ceilometers.

While previous studies have compared various methods of automatically determining sky cover, none has focused on how these instruments compare to each other when sorted into the classification bins that comprise the bulk of the climatological record of sky cover. Therefore, a simple intercomparison between the CEIL and the TSI that simulates as accurately as possible an operational ASOS ceilometer installation was conducted. To mimic standard ASOS observation times, data were taken to produce observations valid at 55 min past the hour, and in order to systematize comparisons done throughout the year, only times that contained enough insolation to produce viable TSI retrievals on every day of the year were used. This resulted in analyses being conducted at hourly intervals from 1455 UTC [0855 central standard time (CST), 0955 central daylight time (CDT)] to 2155 UTC (1555 CST, 1655 CDT). Data were collected from January 2002 through December 2012, resulting in 11 years of analysis. Following Kassianov et al. (2005), the TSI sky cover fraction was taken within a 50° radius of zenith and averaged over the previous 15 min. This was shown to give the best agreement between hemispheric and dense nadir observations of cloud fraction. For both instruments, the data were sorted into the appropriate cloud amount category as would be recorded in an operational METAR observation. The resulting dataset contains over 25 000 paired observations in which both instruments were operational.

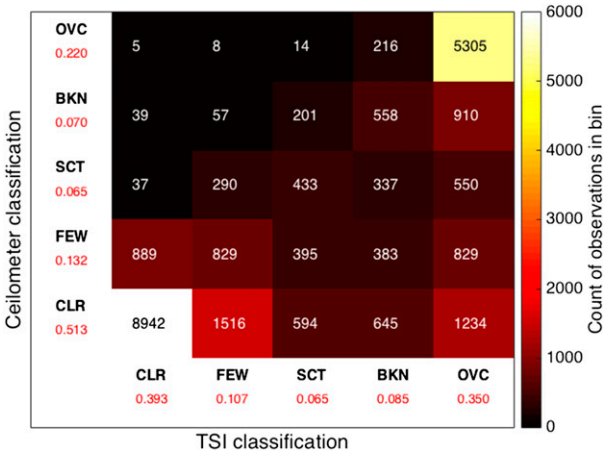

FIG. 1. Intercomparison of sky cover classification as observed by the TSI and the CEIL. The number of observations in each bin is shown, and bins are colored according to the number of observations following the color scale on the right-hand side of the image. Red numbers below each bin identifier represent the fraction of cloud cover classifications observed by each instrument. The color scale is capped at 6000 observations to enhance contrast between intermediate bins.

The two instruments agree broadly; the sky cover fractions exhibit a high degree of correlation with a Pearson correlation coefficient of 0.754. As a result, 82.6% of the observations from one instrument are in the same bin or one bin away from their corresponding observations from the other instrument. However, they do not necessarily agree all that well when examined on the basis of paired bins. Figure 1 shows the number of observations in each paired bin and the percentage of classifications determined by each instrument. For example, the CEIL observed the sky to be clear 51.3% of the time, while the TSI observed clear skies only 39.3% of the time. The values in the bottom row of Fig. 1 can be used to show that 69.2% of the skies that were determined to be clear from the ceilometer were also found to be clear by the TSI, while 9.5% of the clear ceilometer observations were actually found by the TSI to be overcast. In general, one would expect there to be larger values along the ascending diagonal of the figure, indicating significant agreement between the two instruments. In practice, the only categories in which both instruments agree the majority of the time are clear and overcast. This indicates that these automated techniques are likely to agree on cloud cover measurements when the sky is spatially uniform, either completely clear or completely cloudy. Since the skies over the SGP site are typically in either one of these two states (Lazarus et al. 2000), the overall percentage of agreement between the two instruments is high. However, when the sky cover exhibits spatial variability as would be expected with

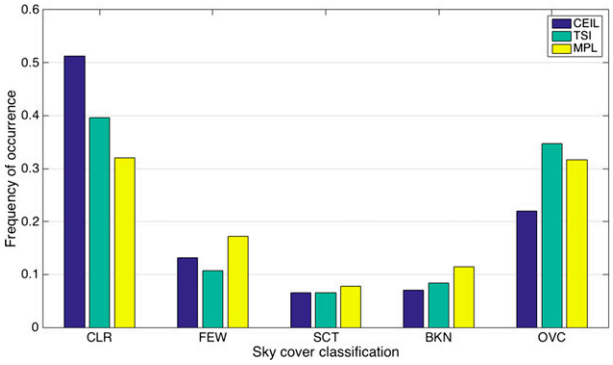

FIG. 2. A climatology of cloudiness as observed at the SGP site for the three instruments analyzed in this work: CEIL (blue), TSI (teal), and MPL (yellow), sorted into the operational sky cover classification bins. Because of limitations of the MPL dataset, this climatology covers only the period between August 2006 and December 2012.

few, scattered, or broken cloud states, these automated methods are not as successful at retrieving consistent measurements. Agreement between the two instruments happened only 27.0% of the time when the ceilometer indicated one of the three variable states (FEW, SCT, or BKN) and only 28.1% of the time that the TSI indicated one of those states.

4. Ceilometer error analysis

Accurate measurements of sky cover from ceilometers rely on three key assumptions. First, it is assumed that the temporal variability in the cloudiness of the zenith view is representative of the spatial variability of the clouds in the sky dome. The second assumption is that skies are clear beyond the vertical range of the ceilometer. Departure from either one of these assumptions will result in a disagreement between the cloud amount observed by the ceilometer and visual sky cover observations. Finally, it is assumed that the recognition of clouds is consistent between observation platforms, an assumption that depends on the instrument's wavelengths, choice of thresholds, range, and sensitivity. The definition of a cloud varies depending on whether one uses a visual, radiometric, or thermodynamic perspective (Wu et al. 2014). Discriminating between these multiple perspectives is a philosophical issue beyond the scope of this paper, so the investigation in this work focuses on the first two assumptions.

Consequently, while different observing systems sited at the same location and observing the same sky will agree broadly, there will often be significant differences between them. This is evident in Fig. 2, which shows a climatology of cloud cover classification bins as observed by the CEIL, TSI, and MPL. All three instruments exhibit the same U-shaped distribution in which CLR or OVC observations are consistently more common than the spatially inhomogeneous bins. However, closer examination shows that the CEIL observation is much more asymmetric than the other two, with a much greater propensity for CLR observations than the other instruments. The likelihood of this being due to differences in the instrument vertical range is discussed in greater detail in section 4b.

It is important to note that sky cover is not necessarily the same as Earth cover, which is the fraction of Earth's surface with clouds directly overhead, or Earth cover observed from a satellite with a nonzero degree look angle (Henderson-Sellers and McGuffie 1990; Genkova et al. 2004; An and Wang 2015). A ceilometer is ultimately attempting to measure Earth cover, as its near-nadir view precludes the observation of cloud sides or clouds that are visible at a distance but will not propagate over the instrument.

a. Point observation error

Sky cover is quantified by evaluating the presence of cloud over two spatial dimensions. A ceilometer is able only to evaluate the presence of cloud at a single location. Averaging the one-dimensional cloud presence variable over time aims to approximate the two-dimensional sky cover quantity. A key assumption with this method is that the temporal inhomogeneity as measured at a single point reflects the spatial inhomogeneity throughout the celestial hemisphere. To determine the accuracy of ceilometer-based observations of sky cover, it is important to evaluate the validity of this assumption.

To isolate the impact of spatial or temporal averaging, synthetic ceilometer observations can be generated directly from the TSI sky images. A small portion of the sky near zenith was evaluated for cloudiness using the operational cloud decision images generated by the TSI. While the TSI algorithm discriminates between thin and opaque clouds, both categories were concentrated into a single cloudy category to mimic the response of the ceilometer. The CEIL has a field-of-view divergence of ± 0.83 mrad, which subtends an area of 0.8 pixels in the low-resolution TSI images (in August 2011, the system was upgraded to include a higher-resolution camera). To reduce pixelated image noise, a 3×3 pixel area was sampled, and the modal value (clear or cloudy) was determined for that spot for every image, captured every 30 s. These observations were then averaged over 30 min, with the most recent 10 min double weighted in accordance with ASOS ceilometer practices. The resulting dataset consists of ceilometer-like observations: near-zenith narrow field-of-view binary determinations of cloud presence. However, since these observations

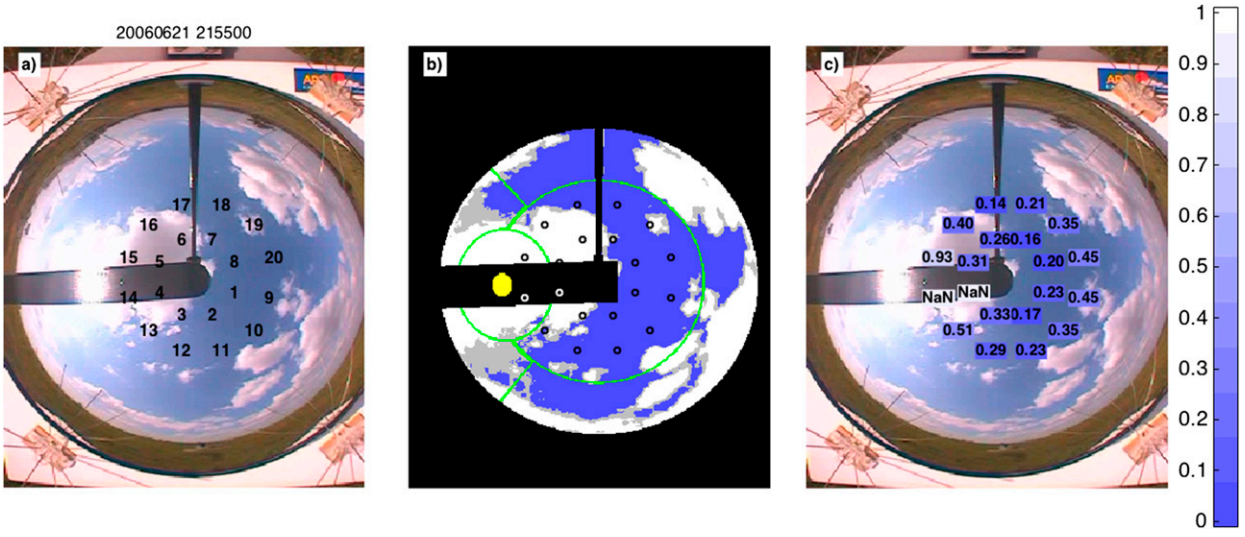

FIG. 3. TSI 2155 UTC 21 Jun 2006. (a) The locations of the 20 spots sampled from the TSI images to create synthetic ceilometer observations, overlaid on a raw TSI image. (b) The TSI cloud mask image product, with blue, gray, and white indicating clear, thin, and opaque clouds, respectively. The green circle around zenith indicates a 100° FOV, and the green circle around the sun indicates a 25° radius. (c) The sky cover fraction averages at the 20 synthetic ceilometer locations, valid for the 30-min period leading up to this image. Spots 4 and 5 and 13–16 lie within 35° of the sun circle. The TSI-calculated hemispheric sky cover is 0.226, whereas the sky cover fraction of synthetic ceilometers beyond 35° of the sun circle range from 0.14 to 0.45 with a mean of 0.272.

were derived directly from TSI imagery, these narrow field temporal averages can be compared directly to the whole-image spatial averages. Since the camera's presence at the direct center of a TSI photograph makes a true zenith view impossible, a distribution of 20 synthetic ceilometers were sampled from the TSI image, as shown in Fig. 3a. There are 8 synthetic ceilometers at a zenith angle of 24°, and 12 synthetic ceilometers at a zenith angle of 45°; north is at the top of the image. The sample image in Fig. 3 is from 2155 UTC 21 July 2006. As this was the summer solstice, this represents the maximum northerly position of the sun for the dates and times of this study. Note that the points 1–4, 9–15, and 20 may be affected by the sun and forward scattering of sunlight near the sun. Figure 3b shows the TSI-derived cloud decision image for this date and time, from which instantaneous values of clear or cloudy were determined for each spot at each 30-s interval. In Fig. 3c the sky cover fraction for each sampled spot is indicated, obtained from a temporal average of the thresholded cloud coverage at each numbered location. Spots falling on the sun strip for more than half the time are withdrawn from analysis. This particular TSI image has an instantaneous sky cover fraction of 0.510 within a 160° field of view (FOV) and 0.322 within a 100° FOV. The 15-min average within a 100° FOV is 0.226. Note that the spot observations that are not near the sun exhibit large variability, with sky cover fraction estimates ranging from 0.14 to 0.45 and a mean of 0.272.

To compare the synthetic ceilometer sky cover fraction observations S_{spot} with hemispheric cloud observations S_{hemis}, a single whole-sky image most consistently represents historical manual observations of cloud cover. However, it is well known that camera sensors incorrectly identify clouds near the sun circle and horizon due to forward scattering and haze. Therefore, the algorithm of Long (2010) is used to correct for the occurrence of haze in these regions, and results comparing S_{spot} to S_{hemis} can be seen in Fig. 4a. Examination of this comparison yields a number of artifacts that can impact cloud detection through digital image processing: 1) spots that occur near the sun circle showed an erroneously high sky cover fraction (Sabburg and Long 2004; Long et al. 2006). Removal of spots that fall within a 35° radius of sun largely removed this effect. 2) The TSI at large zenith view angles is affected by both forward scattering by haze near the horizon and the visibility of cloud sides. Following Kassianov et al. (2005), a 15-min average of TSI-derived sky cover was computed using images captured every 30 s and considering only a 100° FOV. Kassianov et al. determined this product is most consistent with the true earth cover. 3) Some spots showing large differences with the TSI images appeared in images with high-altitude partial cloud cover. The apparent motion of these clouds was not sufficient to create a temporal variability on par with the image spatial variability. Since the ASOS ceilometer does not observe high-altitude clouds, images where the MPL (an instrument discussed in greater detail

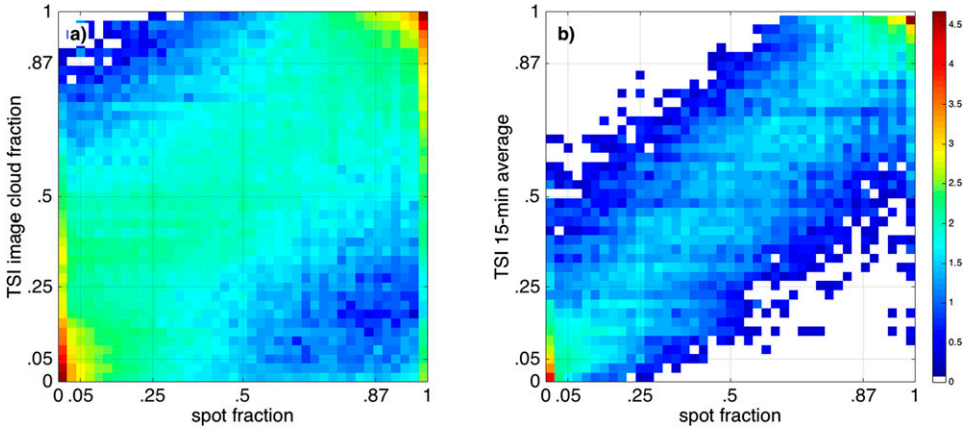

FIG. 4. Joint histograms of all 20 synthetic ceilometers compared with TSI hemispheric observations. (a) The instantaneous TSI image over the whole-sky dome, corrected for haze following Long (2010). There are a total of 429 150 observations and an RMSE of 0.161. (b) The 15-min average of TSI images in a 100° FOV is compared to the spot cloud fraction, after removal of spots that occur within 35° of the sun circle, observations prior to 9 Aug 2006, and observations where the lowest cloud base determined by the MPL is above 3660 m. There are a total of 92 614 observations and an RMSE of 0.0860. Note the logarithmic color scale applies to both panels.

in section 4b) indicated a cloud base above 3660 m were also removed to remove this effect. Because of changes in instrument polarization and processing that may have impacted the determination of cloud-base height from the MPL, only data obtained after 9 August 2006 are used. A comparison of S_{spot} to S_{hemis} after these three adjustments is shown in Fig. 4b. The comparison is strongly improved, with a total root-mean-square error (RMSE) of 0.0860, compared to 0.161 for the entire dataset. The correlation coefficient increased from 0.94 to 0.98, the percentage of observations that fall into the same cloud category increased from 75.1% to 86.5%, and the percentage of observations that fall into the same or adjacent cloud category increased from 94.4% to 99.0%.

The synthetic ceilometer observations were binned into the standard ASOS classes of CLR, FEW, SCT, BKN, or OVC, and normalized distributions of the sky cover fraction difference (TSI minus synthetic ceilometer) for each synthetic ceilometer class is shown in Fig. 5. Because of the low error and therefore narrow distributions for clear and overcast observations, the magnitude of these two distributions was reduced by a factor of 5 to improve visibility in this figure. The scattered cloud cover class is near Gaussian, but the few and broken cloud classes display some skewness.

The RMSE for the synthetic ceilometer compared to the 15-min average 100° FOV TSI sky cover fraction for each of the 20 synthetic ceilometer spots is presented in Fig. 6. The RMSE for spots in the northern half of the TSI image appeared to depend upon the spot zenith angle (red and black lines), whereas spots in the southern half did not (blue and green lines). The variability of RMSE for the spots in the southern half along with larger variability for cloudier categories (BKN and OVC) suggest that the proximity to the sun continues to affect the comparison even after spots within 35° of the

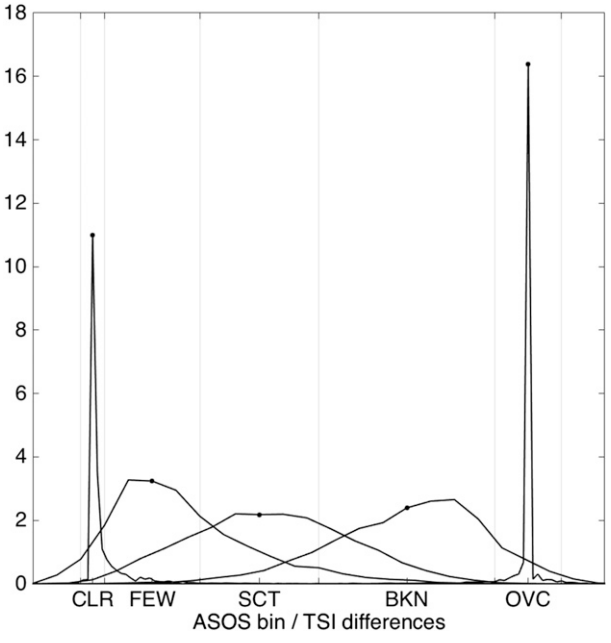

FIG. 5. The probability distributions of the difference (TSI minus synthetic ceilometer) for each of the ASOS bins of sky cover. Note that the clear and overcast distributions have been reduced by a factor of 5 for visibility. The center of each distribution (representing perfect agreement) is indicated with a dot.

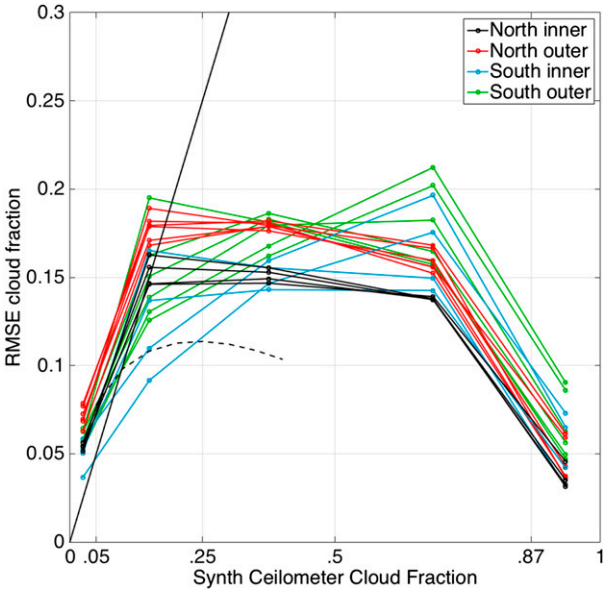

FIG. 6. The RMSE between the synthetic ceilometer observations and the 15-min averaged 50° TSI cloud fraction for each ceilometer cloud fraction class. Dashed line is from Eq. (10) in Berg and Stull (2002), while the solid line is a 1:1 fit; points above the solid line have a greater variability than the signal.

sun were removed. It is concluded that spots sampled from the northern half of the image provide a better representation of true cloudiness due to the relative lack of sun contamination. The synthetic ceilometers sampling at a larger angle from zenith (red lines) show slightly larger RMSE values, suggesting that the visibility of cloud sides or systematic lighting gradients may be at play. Note that the operational TSI threshold that differentiates cloudy from clear pixels is a function of the distance to the image center and the distance to the sun circle, which should correct for any zenithal dependence of sky cover due to image brightness gradients. Berg and Stull (2002) calculated the standard deviation of a one-dimensional sample of a simulated fair weather cumulus cloud field, and derived a functional relationship for the standard deviation as a function of true Earth cover and sample length, which is shown as a black dashed line in Fig. 6. This assumes an averaging length of 18 km, which corresponds to a mean cloud advection speed of 10 m s^{-1} for our averaging time of 30 min. The results shown in the present work are consistent with theirs for clear skies, yet are larger for the few and scattered cloud classes. Berg and Stull focused on fair weather cumulus with a known true cloud fraction, which in all cases was less than 0.4. Henderson-Sellers and McGuffie (1990) showed that observations of Earth cover can be predicted from sky cover observations with an RMSE of roughly one octa from an empirical analysis of ground-based all-sky images. The present study is designed to isolate the effect of spatial and temporal sampling on sky cover estimates by comparing a 100° spatial average to a half-hour temporal average. The variability between the adjusted TSI sky cover and the "true" earth cover could account for Fig. 6's larger variability than Berg and Stull (2002) predict. Boers et al. (2010) found that a narrow (3°) zenith FOV cloud fraction sample resulted in a greater frequency of clear and overcast (0 and 8 octas, respectively) cloud fraction, whereas a full hemispheric FOV increased the occurrence of 1 and 7 octas sky cover, respectively. This result is consistent with the present analysis.

The northern inner radius synthetic ceilometers appear to be least affected by the sun strip and forward scattering of haze near the sun circle and are closest to the zenith observations of the ceilometer. Therefore, the average of synthetic ceilometers 5–8 (black lines in Fig. 6) is assumed to represent the variability of the temporal average of point observations as compared to a spatial average. The average RMSE for each cloud cover class is reported in Table 1. Skies with less than 5% or more than 87% clouds have an RMSE less than 0.06, while partially cloudy conditions show a RMSE of 0.14–0.15. This further reinforces that ceilometers are more successful at observing spatially uniform skies than inhomogeneous skies.

b. High cloud error

To determine the degree that upper-level clouds are not being observed by the ceilometer, the MPL was to create two sets of ceilometer-like sky cover observations: one that uses the full 20-km range of the instrument and another

TABLE 1. A summary of the errors of cloud fraction for the five ASOS cloud fraction classifications due to spatial–temporal averaging error and the presence of clouds above the ceilometer's range of 3660 m.

ASOS category	Original reading	Spatial–temporal averaging error	High cloud error	Total error
CLR	0–0.05	0.054	0.588	0.642
FEW	0.05–0.25	0.153	0.596	0.749
SCT	0.25–0.5	0.151	0.387	0.538
BKN	0.5–0.87	0.138	0.197	0.335
OVC	0.87–1	0.036	0.021	0.057
All clouds	0–1	0.086	0.505	0.591

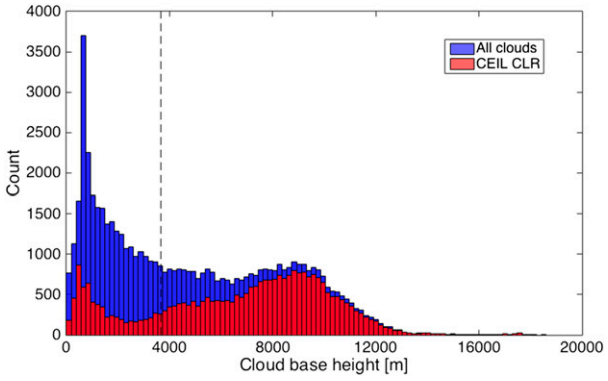

FIG. 7. Histogram of cloud-base height determined by the MPL corresponding to all observations (blue) and observations where the ceilometer observes only clear (0–0.05) skies (red). Mean cloud-base height was obtained by averaging the lowest cloud base as observed by the MPL over a 30-min period with the last 10 min double weighted in order to be consistent with sky cover observations. The vertical dashed line at an altitude of 3660 m corresponds to the upper limit of operational ceilometer observations.

that ignores any cloud with bases in excess of 3660 m. While the MPL was collocated with the ceilometer at the SGP site for the entire duration of the analyzed data, a change in the instrument polarization characteristics in August of 2006 limits the analysis to observations after that time. Since both the ceilometer and the MPL are capable of 24-h operation, sky cover observations were calculated from both instruments once per hour for each hour of the day for the duration of the experimental period; as before the observation time was chosen to be 55 min past the hour in order to mimic the standard synoptic observing schedule. When the MPL observations were modified to be clear when the lowest cloud bases were higher than 3660 m, thus replicating the height limitation of the ceilometer, the sky cover observations from the ceilometer and MPL were in the same classification bin 71.6% of the time and within the same bin or an adjacent one 85.2% of the time. One would not expect the results to be identical as the instruments differ in sensitivities and processing algorithms that determine if a cloud is present. However, when the MPL dataset was expanded to include clouds beyond the height limit of the ceilometer, agreement dropped substantially. Observations were within the same bin only 45.3% of the time and within the same or an adjacent bin 62.6% of the time. The greatest change among all the bins occurred for skies that were found to be clear by the ceilometer yet overcast by the MPL. When looking at the height-restricted dataset, this happened in only 0.51% of all sky observations. However, when looking at the full-height dataset, the frequency of this occurrence increased to 14.1% of all observations. As a result, one can expect significant error in ceilometer-based observations of sky cover when high clouds are present.

The discrepancy between the two instruments is especially stark when one considers only environments where the CEIL observes clear skies. The MPL observes at least some cloudiness in 47.3% of all CEIL clear observations, and 22.8% of the CEIL clear observations are overcast according to the MPL. To ascertain the role that cloud-base height may have in this discrepancy, mean heights for the lowest cloud base present in each MPL observation were calculated using the same weighted temporal average that is used to obtain sky cover. The mean and median cloud-base heights observed by the MPL concurrent with clear observations by the CEIL were 6683 and 7361 m, respectively, far beyond the 3660-m reach of the operational ceilometer network. In fact, 53.9% of all cloud bases observed by the MPL at the SGP site had a base height higher than the ceilometer height limit. This can be seen graphically in Fig. 7, which shows histograms of the cloud-base heights of all MPL-observed clouds (blue) and the cloud-base heights of the MPL-observed clouds when the coincident CEIL observation was clear (red). The dashed vertical line notes the vertical limit of the CEIL dataset. It is clear that as cloud-base heights reach higher into the sky, a greater proportion of the observations are happening in environments where the ceilometer detects no clouds at all, and thus the underestimate of sky cover from the CEIL gets worse. (Note that it is possible for the CEIL to still detect clouds when the mean cloud base is above the 3660-m limit of the instrument; when multiple decks of clouds are present, the CEIL may be observing the lowest layer, while the presence of high clouds results in a mean above the limit.) While the bulk of these higher clouds are ice phase and have little impact on the commercial aviation system for which the ASOS network was designed, the radiative impact of these clouds is significant and any underestimates of cloudiness as a result of insufficient ceilometer range can result in errors in synoptic and climatological forecasts.

Since high clouds are seasonally variable, the discrepancy between the CEIL and MPL will also experience a seasonal change. The fraction of observations for each month that were identical for both instruments was calculated and is shown in Fig. 8a. Agreement was at its lowest in the spring and summer months, reaching a minimum of 38.3% in June. In contrast, agreement is much better for boreal autumn, reaching a maximum of 57.2% in October, coinciding with the climatological minimum in high clouds at the SGP site (Lazarus et al. 2000). The instruments also show greater agreement at night than during the day, as can be seen in Fig. 8b, which also corresponds with the findings of Lazarus et al. (2000) that indicate that high clouds are more prevalent during daytime hours than at night.

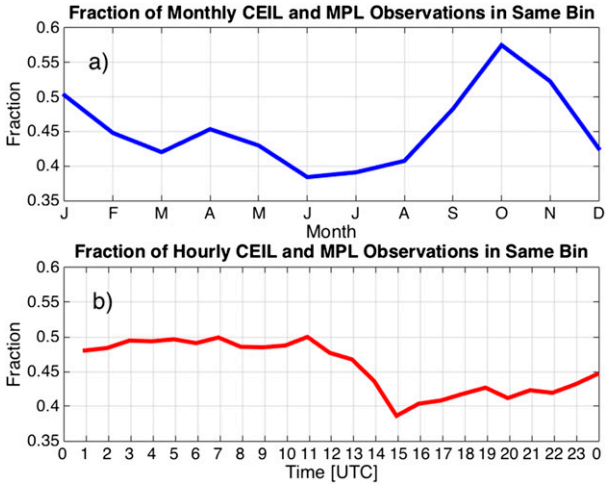

FIG. 8. (a) A monthly climatology of the fraction of cloud cover observations categorized into the same synoptic observation classification by both the ceilometer and the MPL. (b) As in (a), but as an hourly climatology. Note that both charts share the same ordinate range to facilitate direct comparison.

To obtain an estimate of the error induced into ceilometer observations due to the inability to sense high clouds, ceilometer-like sky cover observations were calculated from MPL observations of cloudiness. In essence, the MPL was treated as a very powerful ceilometer that is capable of observing clouds up to and beyond the tropopause. Data were temporally averaged in the standard way for two classes of observations: one in which the entire range of MPL observations were used and one in which clouds above 3660 m were ignored. The sky cover observations from these two datasets were then compared. RMSE calculations of sky cover fraction are shown in Table 1. Agreement was best for overcast skies: when the low-only dataset observes OVC, the cause is almost always thick low stratus clouds that render the inability to observe high clouds moot. As low-level sky cover decreases, opportunities for observations of high-level clouds increase and the discrepancy between the two datasets grows. Agreement is much worse for CLR and FEW observations: the lack of clouds below 3660 m does not preclude the existence of clouds above that level.

5. Conclusions

Ceilometers will be a mainstay of the operational automated weather observation network for years to come. They are relatively inexpensive and require little ongoing maintenance, and are capable of 24-h observations. While TSIs produce automated observations that are qualitatively more similar to human observations of sky cover than the ceilometer, ongoing operational costs like mirror cleaning and reduced hours of operation limit this instrument's applicability for deployment in unattended environments.

Two significant sources of error are associated with the automated sky cover observations obtained by single ceilometer ASOS installations: the spot view of the instrument renders it unable to see the entire sky, while the 3660-m height limit renders the instrument incapable of observing high clouds. These errors are not insignificant, and their magnitudes vary depending on the actual cloud coverage. The spatiotemporal averaging error is smallest for clear and overcast conditions as the sky exhibits little variability in these conditions. The high cloud error is at its smallest when skies are dominated by low clouds, and it tends to increase as low cloud coverage lessens, allowing high clouds to peek through.

Combined error magnitudes are shown in Table 1 alongside the magnitudes of the individual error sources. The least amount of error is present when the sky is overcast. As overcast conditions encompass the whole sky, the variability that causes temporal averaging to differ from spatial averaging is very small. In addition, overcast skies tend to be associated with low clouds, especially stratus clouds, which are well within the viewing range of the ceilometer. As a result, when an ASOS station records an overcast observation, one may have high confidence that such an observation accurately reflects the sky condition at the time. The same cannot be said for other observation values, however. While clear skies are also spatially homogeneous, the inability of the ceilometer to detect high clouds means that a substantial portion of clear-sky observations are actually covered by some fraction of clouds. The most inaccurate classification is FEW as it suffers greatly from both spatial inhomogeneity and susceptibility to high cloud contamination. It is important to note that while the general issues of ceilometer error apply to any installation, the quantitative results apply only to the conditions at the SGP site. Other locations will have climatological variations in high cloud frequency and cloud propagation speed, which will impact the characteristics of the two error sources. Future plans include generalizing this work to other locations where the necessary instruments exist, including other ARM sites and university-based atmospheric research laboratories, to better characterize ceilometer error around the world.

Acknowledgments. Data were obtained from the Atmospheric Radiation Measurement (ARM) data archive, using the sgpceilC1, sgptsiskycoverC1, sgptsiskyimageC1, and sgp30smplcmask1zwangC1 data streams. Support for this work came, in part, from the Creighton University College of Arts and Sciences Summer Faculty Research Fellowship while one of the authors was employed there.

REFERENCES

An, N., and K. Wang, 2015: A comparison of MODIS-derived cloud fraction with surface observations at five SURFRAD sites. *J. Appl. Meteor. Climatol.*, **54**, 1009–1020, doi:10.1175/JAMC-D-14-0206.1.

Berg, L. K., and R. B. Stull, 2002: Accuracy of point and line measures of boundary layer cloud amount. *J. Appl. Meteor.*, **41**, 640–650, doi:10.1175/1520-0450(2002)041<0640:AOPALM>2.0.CO;2.

Boers, R., M. J. de Haij, W. M. F. Wauben, H. K. Baltink, L. H. van Ulft, M. Savenije, and C. N. Long, 2010: Optimized fractional cloudiness determination from five ground-based remote sensing techniques. *J. Geophys. Res.*, **115**, D24116, doi:10.1029/2010JD014661.

Boucher, O., and Coauthors, 2013: Clouds and aerosols. *Climate Change 2013: The Physical Science Basis*. T. F. Stocker et al., Eds., Cambridge University Press, 571–657.

Bretherton, C. S., E. Klinker, A. K. Betts, and J. A. Coakley, 1995: Comparison of ceilometer, satellite, and synoptic measurements of boundary-layer cloudiness and the ECMWF diagnostic cloud parameterization scheme during ASTEX. *J. Atmos. Sci.*, **52**, 2736–2751, doi:10.1175/1520-0469(1995)052<2736:COCSAS>2.0.CO;2.

Cazorla, A., F. J. Olmo, and L. Alados-Arboledas, 2008: Development of a sky imager for cloud cover assessment. *J. Opt. Soc. Amer.*, **25A**, 29–39, doi:10.1364/JOSAA.25.000029.

Dong, X., P. Minnis, and B. Xi, 2005: A climatology of midlatitude continental clouds from the ARM SGP Central Facility: Part I: Low-level cloud macrophysical, microphysical, and radiative properties. *J. Climate*, **18**, 1391–1410, doi:10.1175/JCLI3342.1.

——, B. Xi, and P. Minnis, 2006: A climatology of midlatitude continental clouds from the ARM SGP Central Facility. Part II: Cloud fraction and surface radiative forcing. *J. Climate*, **19**, 1765–1783, doi:10.1175/JCLI3710.1.

Dai, A., T. R. Karl, B. Sun, and K. E. Trenberth, 2006: Recent trends in cloudiness over the United States: A tale of monitoring inadequacies. *Bull. Amer. Meteor. Soc.*, **87**, 597–606, doi:10.1175/BAMS-87-5-597.

Genkova, I., C. N. Long, P. Minnis, P. W. Heck, and M. M. Khaiyer, 2004: Point-to-point comparison of satellite and ground-based cloud properties at the ARM Southern Great Plains Central Facility. *Proc. 14th ARM Science Team Meeting*, Albuquerque, New Mexico, ARM, 18 pp. [Available online at http://www.arm.gov/publications/proceedings/conf14/extended_abs/genkova2-i.pdf.]

Hahn, C. J., S. G. Warren, and J. London, 1995: The effect of moonlight on observation of cloud cover at night, and application to cloud climatology. *J. Climate*, **8**, 1429–1446, doi:10.1175/1520-0442(1995)008<1429:TEOMOO>2.0.CO;2.

Henderson-Sellers, A., and K. McGuffie, 1990: Are cloud amounts estimated from satellite sensor and conventional surface-based observations related? *Int. J. Remote Sens.*, **11**, 543–550, doi:10.1080/01431169008955038.

Kassianov, E., T. Ackerman, R. Marchand, and M. Ovtchinnikov, 2003: Satellite multiangle cumulus geometry retrieval: Case study. *J. Geophys. Res.*, **108**, 4117, doi:10.1029/2002JD002350.

——, C. N. Long, and M. Ovtchinnikov, 2005: Cloud sky cover versus cloud fraction: Whole-sky simulations and observations. *J. Appl. Meteor.*, **44**, 86–98, doi:10.1175/JAM-2184.1.

Koehler, T. L., R. W. Johnson, and J. E. Shields, 1991: Status of the whole sky imager database. *Proceedings of the Cloud Impacts on DoD Operations and Systems (CIDOS-91)*, J. W. Snow and D. D. Grantham, Eds., Science and Technology Corp., 77–80.

Lazarus, S. M., S. K. Krueger, and G. G. Mace, 2000: A cloud climatology of the Southern Great Plains ARM CART. *J. Climate*, **13**, 1762–1775, doi:10.1175/1520-0442(2000)013<1762:ACCOTS>2.0.CO;2.

Liou, K.-N., 1986: Influence of cirrus clouds on weather and climate processes: A global perspective. *Mon. Wea. Rev.*, **114**, 1167–1199, doi:10.1175/1520-0493(1986)114<1167:IOCCOW>2.0.CO;2.

Long, C. N., 2010: Correcting for circumsolar and near-horizon errors in sky cover retrievals from sky images. *Open Atmos. Sci. J.*, **4**, 45–52, doi:10.2174/1874282301004010045.

——, J. M. Sabburg, and J. Calbó, 2006: Retrieving cloud characteristics from ground-based daytime color all-sky images. *J. Atmos. Oceanic Technol.*, **23**, 633–652, doi:10.1175/JTECH1875.1.

Morris, V. R., 2012: Vaisala ceilometer (VCEIL) handbook. ARM Climate Research Facility Tech. Rep. DOE/SC-ARM/TR-020, 18 pp. [Available online at http://www.arm.gov/publications/tech_reports/handbooks/vceil_handbook.pdf.]

Nadolski, V. L., 1998: Automated Surface Observing System (ASOS) user's guide. NOAA, 61 pp.

Pfister, G., R. L. McKenzie, J. B. Liley, A. Thomas, B. W. Forgan, and C. N. Long, 2003: Cloud coverage based on all-sky imaging and its impact on surface solar irradiance. *J. Appl. Meteor.*, **42**, 1421–1434, doi:10.1175/1520-0450(2003)042<1421:CCBOAI>2.0.CO;2.

Rodriguez, D. J., 1998: On the comparability of cloud fractions derived from whole sky imager and ceilometer data. Lawrence Livermore National Laboratory Rep. UCRL-ID-129839, 17 pp.

——, and S. K. Krueger, 1999: Comparisons of cloud cover estimates and cloud fraction profiles from ARM's cloud-detecting instruments and GOES-8 data. *Proc. Ninth ARM Science Team Meeting*, San Antonio, TX, ARM, 8 pp. [Available online at https://www.arm.gov/publications/proceedings/conf09/extended_abs/rodriguez_dj.pdf.]

Sabburg, J., and C. N. Long, 2004: Improved sky imaging for studies of enhanced UV irradiance. *Atmos. Chem. Phys.*, **4**, 2543–2552, doi:10.5194/acp-4-2543-2004.

Schreiner, A. J., K. I. Strabala, D. A. Unger, W. P. Menzel, G. P. Ellrod, and J. L. Pellet, 1993: A comparison of ground and satellite observations of cloud cover. *Bull. Amer. Meteor. Soc.*, **74**, 1851–1861, doi:10.1175/1520-0477(1993)074<1851:ACOGAS>2.0.CO;2.

Shields, J. E., M. E. Karr, R. W. Johnson, and A. R. Burden, 2013: Day/night whole sky imagers for 24-h cloud and sky assessment: History and overview. *Appl. Opt.*, **52**, 1605–1616, doi:10.1364/AO.52.001605.

Stokes, G. M., and S. E. Schwartz, 1994: The Atmospheric Radiation Measurement (ARM) Program: Programmatic background and design of the Cloud and Radiation Test Bed. *Bull. Amer. Meteor. Soc.*, **75**, 1201–1221, doi:10.1175/1520-0477(1994)075<1201:TARMPP>2.0.CO;2.

Wacker, S., and Coauthors, 2015: Cloud observations in Switzerland using hemispherical sky cameras. *J. Geophys. Res. Atmos.*, **120**, 695–707, doi:10.1002/2014JD022643.

Wang, Z., and K. Sassen, 2001: Cloud type and macrophysical property retrieval using multiple remote sensors. *J. Appl. Meteor.*, **40**, 1665–1682, doi:10.1175/1520-0450(2001)040<1665:CTAMPR>2.0.CO;2.

WMO, 1975: *Manual on the Observation of Clouds and Other Meteors*. Vol. 1, *International Cloud Atlas*, WMO-407, 155 pp.

Wu, W., Y. Liu, M. P. Jensen, T. Toto, M. J. Foster, and C. N. Long, 2014: A comparison of multiscale variations of decade-long cloud fractions from six different platforms over the Southern Great Plains in the United States. *J. Geophys. Res. Atmos.*, **119**, 3438–3459, doi:10.1002/2013JD019813.